Environmental Science and Pollution Research (2019) 26:18893–18903
https://doi.org/10.1007/s11356-019-05119-9

SHORT RESEARCH AND DISCUSSION ARTICLE

Synthesis of novel sepiolite–iron oxide–manganese dioxide nanocomposite and application for lead(II) removal from aqueous solutions

Maryam Fayazi[1] · Daryoush Afzali[1] · Reza Ghanei-Motlagh[2] · Aida Iraji[3]

Received: 31 December 2018 / Accepted: 8 April 2019 / Published online: 10 May 2019

Abstract

In this study, the sepiolite–iron oxide–manganese dioxide (Sep–Fe_3O_4–MnO_2) nanocomposite was synthesized and applied as a magnetically separable adsorbent for removal of Pb(II) ions from water in a batch system. The effects of initial Pb(II) concentration, adsorbent dosage, contact time, pH value, and temperature were investigated to optimize the conditions for maximum adsorption. The equilibrium adsorption data were analyzed with the Langmuir, Freundlich, and Temkin models. The adsorption process closely agreed with the Langmuir adsorption isotherm, and the monolayer saturation adsorption value was achieved as 131.58 mg g^{-1}. The adsorption kinetics follow the pseudo-second-order (PSO) model that illustrated the rate controlling step might be chemisorption. Thermodynamic investigations for the removal process were conducted by determining the values of $\Delta G°$, $\Delta H°$, and $\Delta S°$. The adsorption behavior of Pb(II) on the Sep–Fe_3O_4–MnO_2 was a spontaneous and endothermic process. Several consecutive adsorption–desorption cycles confirmed that the proposed Sep–Fe_3O_4–MnO_2 nanocomposite could be reused after successive lead removal. Furthermore, the practical application of the adsorbent was successfully realized by the treatment of real Pb-contaminated water samples.

Keywords Removal · Manganese dioxide · Sepiolite · Magnetic adsorbent · Lead

Introduction

In recent years, environmental contamination by heavy-metal ions has become a serious environmental problem due to non-biodegradability, accumulation in living body, discharge, and high toxicity of these heavy metals. The main pathway through which heavy metals enter the environment is via wastes from industrial activities such as mining, metallurgical, tannery, painting, and battery manufacturing industries (Fu and Wang 2011). Lead (Pb) is one of the common and toxic heavy metals released into the environment water samples (Wang et al. 2013). Today, the exploring of reliable, efficient, and cost-effective removal of lead from water/wastewater is considered very important. Recently, various methods have been presented for the treatment of lead consisting of chemical precipitation (Matlock et al. 2002), electrochemical method (Liu et al. 2013), biological method (Bowman et al. 2018), ion exchange (Chanthapon et al. 2018), membrane filtration (Choudhury et al. 2018), and adsorption processes (Ali 2012). Among them, adsorption is a conventional and efficient technique for the removing of Pb(II) ions from water/wastewater because of the convenience in design, economic viability, sludge-free operation properties, and regeneration capability of the adsorbents (Ghorbani et al. 2018). Thus, developing

Responsible editor: Tito Roberto Cadaval Jr

Electronic supplementary material The online version of this article (https://doi.org/10.1007/s11356-019-05119-9) contains supplementary material, which is available to authorized users.

✉ Maryam Fayazi
maryam.fayazi@yahoo.com; m.fayazi@kgut.ac.ir

[1] Department of Environment, Institute of Science and High Technology and Environmental Sciences, Graduate University of Advanced Technology, Kerman, Iran

[2] Department of Clinical Sciences, Faculty of Veterinary Medicine, Shahid Chamran University of Ahvaz, Ahvaz, Iran

[3] Central Research Laboratory, Shiraz University of Medical Sciences, Shiraz, Iran

novel adsorbents with high capacity, easy separation, and stable efficiency is highly desired (Guo et al. 2018; Nqombolo et al. 2019).

Sepiolite (Sep), $Si_{12}Mg_8O_{30}(OH)_4(OH2)_4{\cdot}8H_2O$, is a fibrous clay mineral with molecular-sized channels (Zhang et al. 2018). Considering its large surface area, high porosity, natural abundance, and the silanol-based chemistry of the surface, sepiolite exhibits exceptional adsorption capability for heavy-metal ions (Celis et al. 2000; Lazarević et al. 2007). However, its relatively low adsorption capacity and difficult separating from the aqueous solutions seriously limits application of the natural sepiolite in water treatment (Fu et al. 2015).

Recently, magnetic materials as efficient adsorbents have been utilized for heavy-metal treatment due to low toxicity, large specific surface area, and superparamagnetic property (Giraldo et al. 2013). Magnetic sepiolite composites are very promising as novel materials for application in water treatment due to easy isolation from the aqueous phase by applying an external magnetic field (Tian et al. 2015; Yu et al. 2016). Nevertheless, a lot of magnetic adsorbents used for heavy-metal removal exhibit low adsorption capacity. In order to meet the requirement of higher adsorption capacity, one effective strategy is the integration of transition metal oxides into magnetic sepiolite composite.

Among transition metal oxides, manganese oxides, with the advantages of low-cost, natural abundance, high adsorption efficiency for heavy metals, and environmental friendliness, appear to be a promising material in sorption studies (Qin et al. 2011; Tripathy et al. 2006). Tan et al. used MnO_x-coated rice straw biochar (RSB) for efficient adsorption of Pb(II) with good reusability (Tan et al. 2018). The obtained RSB/MnO_x composite shows extraordinary adsorption capacity for removal of lead ions as compared with unmodified RSB. Xiang et al. (2017) employed flower-like nickel ferrite/manganese dioxide ($NiFe_2O_4/MnO_2$) composite for lead removal that was obtained with a facile hydrothermal method. In a previous study, we modified the magnetic halloysite nanotubes with wire-like MnO_2 via hydrothermal method (Afzali and Fayazi 2016). This magnetic material is found to be an ideal adsorbent for lead removal with effective treatment.

Inspired by these studies, we designed and prepared a new magnetically recoverable nanocomposite (Sep–Fe_3O_4–MnO_2) for enhanced lead removal from aqueous solutions, by virtue of the synergy of Fe_3O_4 and MnO_2. The morphology and structure of the prepared Sep–Fe_3O_4–MnO_2 nanocomposite was well characterized by X-ray diffraction (XRD), Fourier transform infrared spectroscopy (FT-IR), vibrating sample magnetometer (VSM), transmission electron microscopy (TEM), and Brunauer–Emmett–Teller (BET) analysis. The critical factors which affect the adsorption process, such as contact time, Sep–Fe_3O_4–MnO_2 dose, solution pH, initial concentration, and temperature, have been systematically investigated. Kinetic, equilibrium, and thermodynamic investigations have also been discussed in detail. This study can potentially be employed for the efficiency improvement in lead ion treatment and demonstrates superior to other magnetic sorbents for this purpose.

Experimental

Materials

Raw sepiolite material (≤ 0.075 mm) obtained from Fariman in Iran was used in this work. The main chemical composition of the mineral sample (in percent weight) consisted of 53.92 SiO_2, 0.21 Al_2O_3, 0.01 Fe_2O_3, 2.94 CaO, 0.01 Na_2O, 0.01 K_2O, 24.22 MgO, and 18.68 loss of ignition (LOI). Lead(II) standard solution (1000 mg L^{-1}) was prepared by dissolving proper amounts of lead nitrate ($Pb(NO_3)_2$) (Sigma-Aldrich Co., St. Louis, MO, USA) in deionized water. Chemicals including potassium permanganate ($KMnO_4$), ethylenediaminetetraacetic acid (EDTA), ferrous chloride tetrahydrate ($FeCl_2{\cdot}4H_2O$), ammonium hydroxide (NH_4OH, 25 % *w*/*w*), and ammonium persulfate ($(NH_4)_2S_2O_8$) were acquired from Merck (Darmstadt, Germany).

In order to purify raw Sep, 5 g of mineral sample was suspended in 500 mL of distilled water. The suspension was mechanically stirred for 24 h according to the literature method (Doğan et al. 2008). After waiting for about 2 min, the suspended solid particles were filtered through a filter paper. The filtered sample was then dried overnight at 105 °C to obtain purified Sep.

The Sep–Fe_3O_4 nanocomposite was prepared via hydrothermal method. Firstly, 2.5 g of purified sepiolite was added to 40 mL solution of 6.5 g $FeCl_2{\cdot}4H_2O$ and stirred for 10 min at air condition, allowing the iron(II) to be oxidized. Then, 31 mL of NH_4OH solution was added under vigorous agitation. The black suspension was taken and transferred into a Teflon-lined autoclave (200-mL capacity) and then kept in an oven at 145 °C for 5 h. Afterward, the product was separated by a magnetic attraction and then washed repeatedly with double-distilled water. Finally, the Sep–Fe_3O_4 product was dried at 60 °C for 24 h.

The Sep–Fe_3O_4–MnO_2 nanocomposite was also prepared by hydrothermal process. For this purpose, 4.2 g of the Sep–Fe_3O_4 nanocomposite was dispersed into 60 mL mixed solution of $(NH_4)_2S_2O_8$ (4.42 g) and $KMnO_4$ (3.70 g) for 15 min. The mixture solution was then sealed in a Teflon-lined stainless-steel autoclave and heated at 110 °C for 14 h. The achieved Sep–Fe_3O_4–MnO_2 material was isolated by a magnet, followed by repeated washing with distilled water, and dried in an oven at 60 °C.

Equipment

Lead content of solutions was determined by a Varian model AA-220 flame atomic absorption spectrometer (FAAS, Varian, Musgrave, Australia). The infrared spectra were measured on a Nicolet AVATARIR 360 spectrometer (Thermo Electron Corporation, Madison, WI, USA) using a pressed KBr tablet method. All N_2 adsorption/desorption experiments were conducted on an Autosorb-1MP system (Quantachrome Instruments, Boynton Beach, FL, USA). XRD patterns of the prepared materials were evaluated using Cu Kα radiation (λ = 1.542 Å) on a PANalytical powder diffractometer X'Pert PRO (PANalytical B.V., Almelo, The Netherlands). TEM analysis was performed with Tecnai G2 F20 S-TWIN (FEI, USA). The saturation magnetization of the sample was determined with a VSM instrument Model LDJ9600 (LDJ Electronics Co., USA). The speciation of Pb(II) was acquired using the chemical speciation software Visual MINTEQ (Version 3.0).

Adsorption experiments

The lead adsorption experiments were conducted using a batch mode by adding the adsorbents to a 20 mL Pb(II) solution (in 50-mL Erlenmeyer flasks) at the desired pH. The mixture was gently shaken for a desired contact time at 200 rpm to attain adsorption equilibrium. Finally, the adsorbent was separated and the residual concentration of lead ions in supernatant fluid was analyzed with FAAS technique.

The equilibrium adsorption capacity (q_e, mg g^{-1}) and removal efficiency (R, %) were calculated by the following equations:

$$q_e = \frac{C_i - C_e}{m} \times V \quad (1)$$

$$R = \frac{C_i - C_e}{C_i} \times 100 \quad (2)$$

where C_i (mg L^{-1}), C_e (mg L^{-1}), V (L), and m (g) are the initial lead ion concentration, equilibrium lead ion concentration, the volume of lead solution, and mass of dry adsorbent, respectively.

Results and discussion

Characterization

FT-IR spectra for the Sep, Sep–Fe_3O_4, and Sep–Fe_3O_4–MnO_2 nanocomposite are depicted in Fig. S1. The bands and lattice vibrations in FT-IR spectrum of Sep can be summarized as follows: 3567 cm^{-1} and 3418 cm^{-1} to the O–H stretching vibration of the variant H_2O molecules existing in the Sep sample; 1662 cm^{-1} to the hydroxyl bending mode of zeolitic water; 974 cm^{-1}, 1079 cm^{-1}, and 1209 cm^{-1} to the Si–O bands vibration (Tabak et al. 2009); 1016 cm^{-1} to the Si–O–Si plane vibration; and 646 cm^{-1} to the Mg–OH bending vibration (Cornejo and Hermosin 1988). In the Sep–Fe_3O_4 spectrum, the band located at around 1091 cm^{-1} is due to the Si–O–Fe linkage and another band at around 570 cm^{-1} corresponds to stretching vibration of Fe–O bond (Chandra et al. 2010), respectively. In comparison, the Sep–Fe_3O_4–MnO_2 has two new absorption bands than Sep–Fe_3O_4. The bands observed at 509 cm^{-1} and 1420 cm^{-1} are assigned to the bending vibration Mn–O bond (Li et al. 2007) and bending vibration of MnO–H groups (Du et al. 2014), respectively.

The morphology of the Sep, Sep–Fe_3O_4, and Sep–Fe_3O_4–MnO_2 was characterized by TEM as indicated in Fig. 1. It is evident that the mineral sepiolite sample has a fibrillar structure (Fig. 1a) and the spherical Fe_3O_4 nanoparticles are well placed on its surface (Fig. 1b). From the TEM image of the Sep–Fe_3O_4–MnO_2 (Fig. 1c), it is obviously seen that a large amount of interconnected MnO_2 nanoflakes completely deposited on the surface of the Sep–Fe_3O_4 nanocomposite.

The XRD patterns of the Sep, Sep–Fe_3O_4, and Sep–Fe_3O_4–MnO_2 are illustrated in Fig. 1d. The appeared diffraction peaks at 2θ = 19.9° (060), 20.8° (131), 24.0° (260), 26.8° (080), 28.2° (331), 35.2° (371), 26.8° (202), and 40.1° (451) can be indexed to the characteristic peaks of sepiolite (JCPDS, No. 13-0595) (Liu and Chen 2015). The presence of Fe_3O_4 nanoparticles are indicated by the main diffraction peaks at 2θ = 30.5° (220), 35.8° (311), 43.6° (400), 54.1° (422), 57.6° (511), and 63.0° (440). The obtained patterns match with inverse spinel structure of magnetite (JCPDS, No. 19-0629) (Zhang et al. 2015). Furthermore, the diffraction peaks at 2θ = 37.3° (131) and 66.3° (421) may be due to the birnessite type of γ-MnO_2 according to JCPDS No. 14-0644 (He et al. 2017). Besides, the characteristic peaks of Sep and Sep–Fe_3O_4 samples cannot be found in the Sep–Fe_3O_4–MnO_2 pattern. This is probably because of high chemical deposition of MnO_2 on Sep–Fe_3O_4 composite.

The magnetic hysteresis curves of the Sep–Fe_3O_4 and Sep–Fe_3O_4–MnO_2 nanocomposite at room temperature are exhibited in Fig. 1e. The Sep–Fe_3O_4 composite indicates the typical superparamagnetic property. The saturation magnetization (M_s) of the Sep–Fe_3O_4 was found to be 28.1 emu g^{-1}. Moreover, the M_s value of the Sep–Fe_3O_4–MnO_2 nanocomposite was obtained as 8.9 emu g^{-1}, which is lower than that of the Sep–Fe_3O_4 sample. The decrease of the M_s value can be mainly attributable to deposition of MnO_2 nanoflakes. In addition, the prepared Sep–Fe_3O_4–MnO_2 nanocomposite responds well to the magnetic field, which favors the magnetic adsorption of pollutants.

The N_2 adsorption/desorption isotherms of different sorbent materials (Sep, Sep–Fe_3O_4, and Sep–Fe_3O_4–MnO_2) are displayed in Fig. 1f. The IV type adsorption–desorption

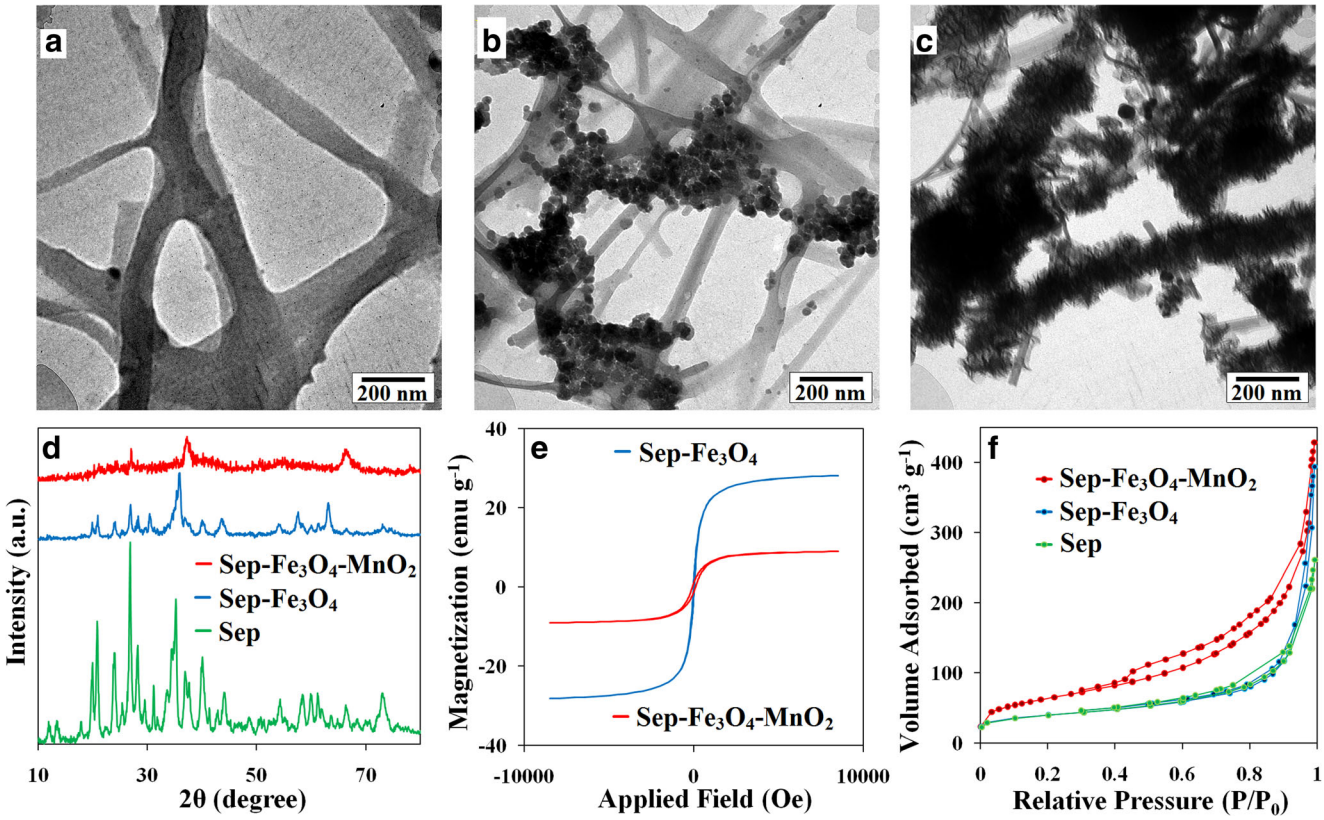

Fig. 1 TEM images of **a** Sep, **b** Sep–Fe_3O_4, and **c** Sep–Fe_3O_4–MnO_2 nanocomposite. **d** XRD patterns, **e** magnetization curves, and **f** N_2 adsorption/desorption isotherms of Sep, Sep–Fe_3O_4, and Sep–Fe_3O_4–MnO_2

isotherm of mesoporous materials (Barrett et al. 1951) is observed for all samples. The BET-specific surface areas of the natural Sep, Sep–Fe_3O_4, and Sep–Fe_3O_4–MnO_2 are 137.5 m^2 g^{-1}, 138.2 m^2 g^{-1}, and 223.0 m^2 g^{-1}, respectively, and the corresponding pore volumes are 0.38 cm^3 g^{-1}, 0.57 cm^3 g^{-1}, and 0.62 cm^3 g^{-1}. Consequently, the specific surface area of the Sep–Fe_3O_4 composite increased after being covered with MnO_2 nanoflakes.

Effective parameters on lead removal

pH effect

In the adsorption of metal ions from aqueous solutions, pH is one of the vital parameters that affect the adsorbent surface characteristics and adsorbate solubility (Zhou et al. 2013). Therefore, the influence of pH on adsorption of lead(II) ions on the Sep–Fe_3O_4–MnO_2 nanocomposite was investigated. The experiment was performed at pH ranged from 3.0 to 9.0 and room temperature (23 ± 2 °C) by shaking 0.04 g of the adsorbent with a solution of 100 mg L^{-1} (20 mL) Pb(II) for 60 min at 200 rpm. As depicted in Fig. 2a, the maximum adsorption occurs at pH 6.0 to 9.0. When pH is less than 6.0, the uptake of lead ions is lower probably due to the competition between hydrogen and lead ions on the active surface sites of adsorbent (Xu et al. 2008). Generally, the adsorption of metal cations is highly favored at pH > pH of zero point charge (pH_{zpc}) (Babić et al. 2002). The pH_{zpc} value of γ-MnO_2 is about 5.5 (Koulouris 1995); thus, the negatively charged surface of MnO_2-based composite can be observed at pH > 5.5. On the other hand, the main species of Pb(II) in aqueous solutions are Pb^{2+}, $Pb(OH)^+$, $Pb(OH)_2$, and $Pb(OH)_3^-$ at various pH values (Fig. 2b). The main species of lead at pH 6–8 are $Pb(OH)^+$ and Pb^{2+}, and thus the removal of lead can be caused by the electrostatic attraction between negatively charged Sep–Fe_3O_4–MnO_2 surface and these positively charged species. Above pH 8.0, the adsorption of lead is mainly attributable to the mixed effect of adsorption and formation of insoluble lead hydroxide ($Pb(OH)_2$). Moreover, the variation of solution pH values before and after the adsorption process was explored in order to understand the adsorption mechanism. As seen in Fig. 2c, the solution pH decreased a little to the acidic region after the adsorption process. These results indicated that upon the electrostatic interaction, complexation and ion exchange could also occur in the lead sorption process at pH 6.0.

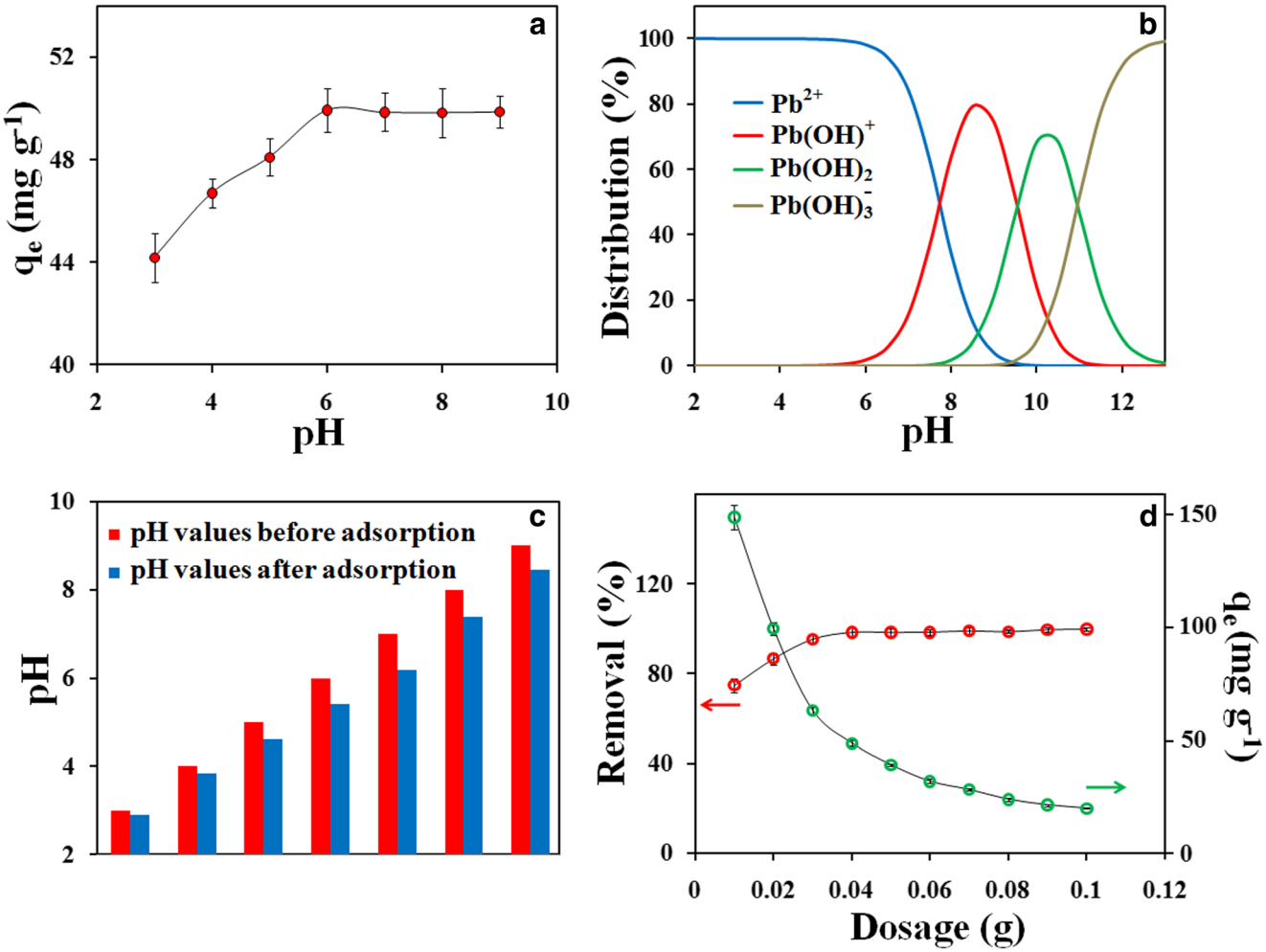

Fig. 2 **a** Effect of pH on adsorption of Pb(II) by Sep–Fe_3O_4–MnO_2. **b** Distribution of Pb(II) species in aqueous solutions as a function of pH. **c** Comparison of solution pH values before and after adsorption process. **d** Effect of adsorbent dosage on the Pb(II) removal efficiency

Ionic strength effect and removal mechanism

The influence of ionic strength on the adsorption behavior of Pb(II) by the prepared magnetic nanocomposite was also studied. It has been documented that the ionic strength can be employed to predict the adsorption mechanism (Hayes and Leckie 1987). The ionic strength can influence the thickness of double layer and the interfacial potential, thereby, can affect the binding of the adsorbed species. As shown in Fig. S2, the adsorption capacities of Pb(II) decrease with an increase in the ionic strength of the electrolyte ($NaClO_4$) solution, which could be attributed to the competitive effect between lead ions and salt cations for the available adsorption sites. In general, outer-sphere surface complexation and ion exchange are expected to be more vulnerable to ionic strength variations than inner-sphere surface complexation (Yang et al. 2011). The ionic strength and pH-dependent adsorption by the MnO_2-based sorbent shows that the adsorption mechanism is ion exchange or outer-sphere surface complexation (through electrostatic binding reaction) rather than inner-sphere complexation (Duan et al. 2015). By taking into account the above results, the mechanism of the specific surface reactions can be expressed as follows (Han et al. 2006; Zhao et al. 2016):

$$\equiv MnOH + Pb^{2+} \rightarrow \equiv MnOPb^{+} + H^{+} \text{ (ion exchange)}$$
$$\equiv MnO^{-} + Pb^{2+} \rightarrow \equiv MnO^{-}Pb^{2+} \text{ (electrostatic attraction)}$$
$$2(\equiv MnOH) + Pb^{2+} \rightarrow (\equiv MnO)_2Pb + 2H^{+} \text{ (ion exchange)}$$
$$2(\equiv MnO^{-}) + Pb^{2+} \rightarrow (\equiv MnO^{-})_2Pb^{2+} \text{ (electrostatic attraction)}$$

Adsorbent dosage effect

The influence of adsorbent mass on the adsorption capacity and capturing performance was carried out by conducting a series of experiments with varying amount of Sep–Fe_3O_4–MnO_2 (0.01–0.1 g), and the results are shown in Fig. 2d. It is obvious that the removal percentage of lead ions increases

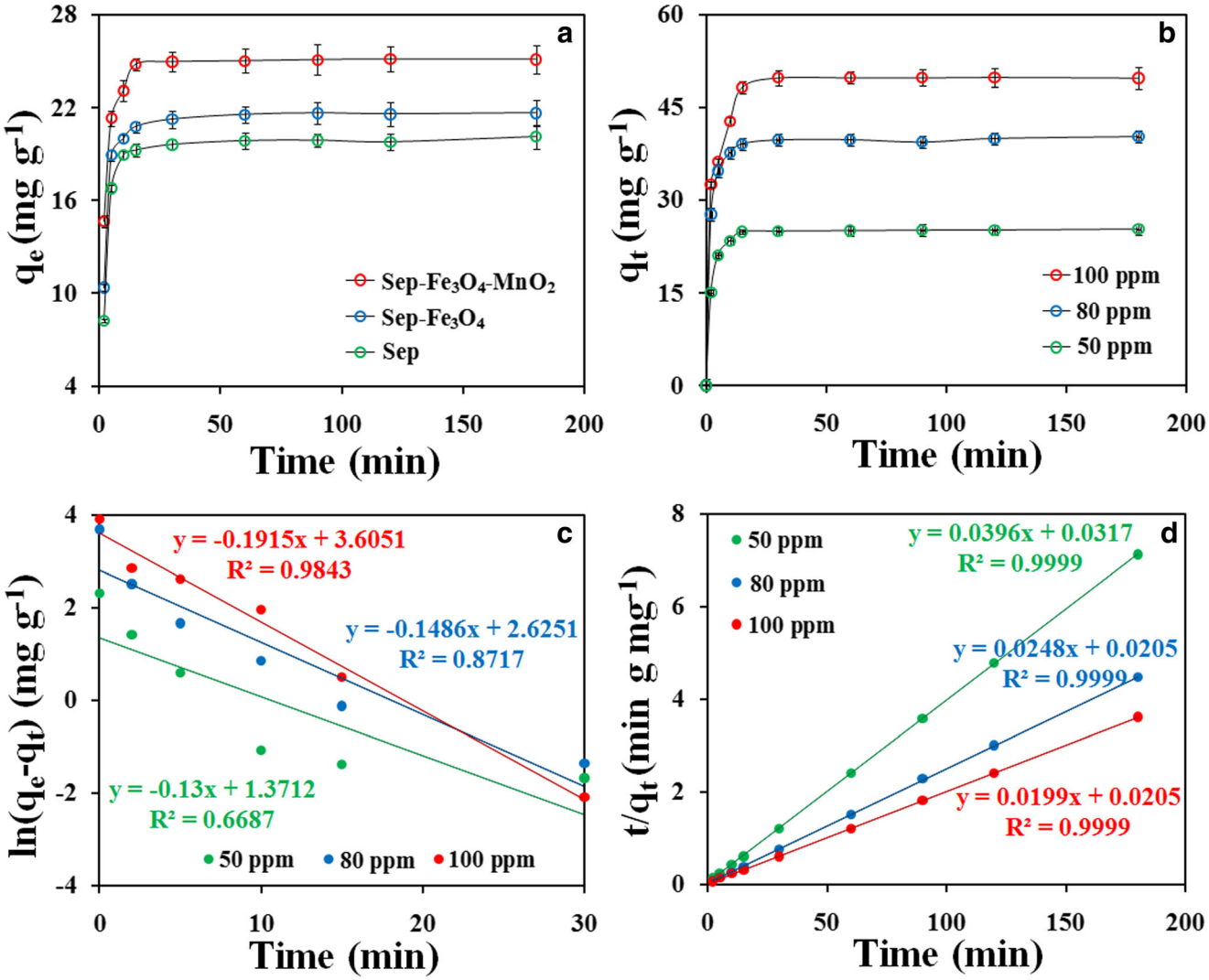

Fig. 3 **a** Effect of contact time on adsorption of Pb(II) by Sep, Sep–Fe_3O_4, and Sep–Fe_3O_4–MnO_2 nanocomposite. **b** Adsorption capacity versus adsorption time at various initial Pb(II) concentrations. **c** Pseudo-first-order and **d** pseudo-second-order models fitting for Pb(II) adsorption by Sep–Fe_3O_4–MnO_2 nanocomposite

with increasing the Sep–Fe_3O_4–MnO_2 nanocomposite in solution up to 0.04 g, and tends to reach steady at the higher amount. This may be due to the availability of more active sites for adsorption of Pb(II) with increasing the adsorbent dosage (Arshadi et al. 2014). In contrast, the adsorption capacity decreased with increasing the sorbent content. The progressive decrease in the adsorption capacity at high dosage is owing to increasing the number of the unsaturated adsorption sites on the adsorbent (Sharma et al. 2014). So, adsorbent amount of 0.04 g was selected for subsequent experiments.

Effect of contact time and initial adsorbate concentration

Figure 3a illustrates the effect of contact time on the adsorption capacity after treatment of 50 mg L^{-1} Pb(II) solution (20 mL) with the optimum dosage (0.04 g) of the natural SEP, Sep–Fe_3O_4, and Sep–Fe_3O_4–MnO_2 at pH = 6.0 for comparison. As it is visualized in Fig. 3a, the adsorption capacity of the Sep–Fe_3O_4–MnO_2 increased with reaction time during the first 15 min and remained almost constant at higher contact times as equilibrium was reached, while Pb(II) uptake of the SEP and Sep–Fe_3O_4 sorbents increased with the time during the first 30 min and it became much slower and finally attained equilibrium within 60 min. The faster adsorption rate of the Sep–Fe_3O_4–MnO_2 compared to the SEP and Sep–Fe_3O_4 is because of the availability of a large number of MnO_2 nanoflakes with high affinity towards lead ions.

Furthermore, the effect of reaction time and initial lead concentration on the adsorption capacity of the Sep–Fe_3O_4–MnO_2 nanocomposite is demonstrated in Fig. 3b. It is evident that the sorption ability of Pb(II) ions demonstrates a concentration-dependent character. The adsorption capacity of the Sep–Fe_3O_4–MnO_2 increases with increasing the initial Pb(II) concentration. The reason might be the fact that the

Table 1 Kinetic parameters for Pb(II) adsorption on Sep–Fe_3O_4–MnO_2 nanocomposite at various concentrations

C_0 (mg L^{-1})	$q_{e,\ exp}$ (mg g^{-1})	PFO model			PSO model		
		$q_{e,\ cal}$ (mg g^{-1})	k_1 (min^{-1})	R^2	$q_{e,\ cal}$ (mg g^{-1})	k_2 (g mg^{-1} min^{-1})	R^2
50	25	3.94	0.130	0.6687	25.3	0.050	0.9999
80	39.7	14.05	0.147	0.8717	40	0.047	0.9999
100	49.7	32.60	0.202	0.9843	50.25	0.020	0.9999

mass transfer driving force would become larger at higher initial adsorbate concentration (Tan et al. 2008). Moreover, the obtained results indicate that the equilibrium time increases with the initial Pb(II) concentration.

Adsorption kinetics

For evaluation of the adsorption kinetics, the pseudo-first-order (PFO) and the pseudo-second-order (PSO) kinetic models were used (Fayazi et al. 2015). The details of the two kinetic models used in this study are described in the Supplementary Information and the fitting results are shown in Fig. 3 panels c and d and Table 1. It should be noted that experimental data can be fitted with the PSO kinetics model with correlation coefficients (R^2) greater than 0.999, suggesting that the adsorption of lead(II) ions by the magnetic Sep–Fe_3O_4–MnO_2 nanocomposite occurs through chemical adsorption.

Adsorption isotherms

Different mathematical models (Langmuir, Freundlich, and Temkin) have been employed to evaluate the adsorption

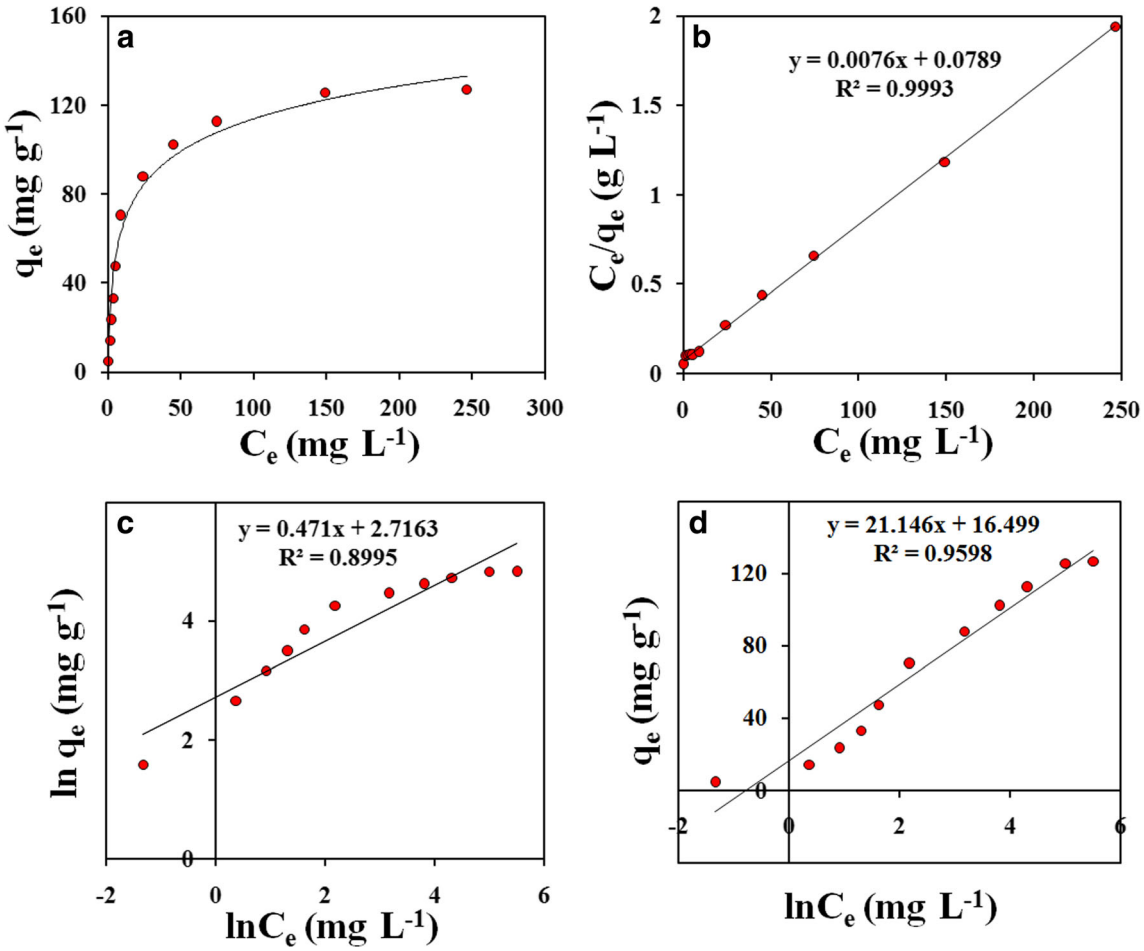

Fig. 4 **a** Equilibrium adsorption isotherm of Pb(II) on Sep–Fe_3O_4–MnO_2. **b** Langmuir model, **c** Freundlich model, and **d** Temkin model fittings for Pb(II) adsorption by Sep–Fe_3O_4–MnO_2 nanocomposite

Table 2 Langmuir, Freundlich, and Temkin isotherm parameters of Pb(II) adsorption

Langmuir isotherm		
K_L (L mg^{-1})	q_m (mg g^{-1})	R^2
0.0963	131.58	0.9993
Freundlich isotherm		
K_F (mg g^{-1} (L mg^{-1})$^{1/n}$)	n	R^2
15.12	2.123	0.8995
Temkin isotherm		
B_T	A_T (L mg^{-1})	R^2
21.146	2.18	0.9598

isotherms (Luk et al. 2017). Detailed descriptions of these models are described in the Supplementary Information. The results of the isotherms were derived by analyzing Fig. 4 and the corresponding isotherm parameters are listed in Table 2. According to the R^2 values, the Langmuir isotherm displayed a better fit for the adsorption data than other isotherm models. The Langmuir adsorption manner implies the monolayer adsorption of lead ions onto a homogeneous surface of the magnetic sorbent (Wei et al. 2017). Moreover, the theoretical maximum adsorption capacity is 131.58 mg g^{-1}, approaching the experimental value (126.82 mg g^{-1}). Table 3 lists the adsorption capacity of the current adsorbent with other reported materials (Afzali and Fayazi 2016; Bo et al. 2015; Eren 2009; Eren and Gumus 2011; Gabris et al. 2018; Karaoğlu et al. 2013; Liang et al. 2011; Salam 2013; Xiang et al. 2017; Yang et al. 2013; Yu et al. 2018; Zou et al. 2018; Zou et al. 2006) for lead(II) treatment. As it is visualized in the table, the adsorption capacity of the Sep–Fe_3O_4–MnO_2 is comparable with or, in most cases, higher than the other reported adsorbents. Therefore, the proposed magnetic sorbent is very promising for the efficient removal of lead in environmental remediation.

In addition, the dimensionless separation factor (R_L, see the Supplementary Information) estimated from the Langmuir adsorption isotherm was found between 0 and 1 for all tested lead concentrations (Table S1), thereby confirming that the removal of Pb(II) ions on the magnetic Sep–Fe_3O_4–MnO_2 nanocomposite is a favorable process (Chegrouche et al. 2009).

Adsorption thermodynamic parameters

In order to fully understand the adsorption process of lead (II) onto the Sep–Fe_3O_4–MnO_2, the changes in thermodynamic including standard Gibbs free energy (ΔG°), standard enthalpy (ΔH°), and standard entropy (ΔS°) were evaluated (Mallakpour and Behranvand 2017). For detailed information, see the Supplementary Information. A summary of the calculated thermodynamic parameters is given in Table 4. The negative values of ΔG° indicate that Pb(II) adsorption on Sep–Fe_3O_4–MnO_2 nanocomposite is a spontaneous process. The negative values of ΔG° at the higher temperature imply that a better Pb(II) adsorption can be achieved at the higher temperature. Moreover, the positive values of ΔH° and ΔS° also imply the endothermic nature of adsorption and the increase in randomness at the solid/solution interface, respectively (Karthik and Meenakshi 2015).

Table 3 Comparative study of different adsorbents for Pb(II) adsorption

Adsorbents	Adsorption capacity (mg g^{-1})	pH	Refs.
3D hierarchical flower-like nickel ferrite/manganese dioxide	85.78	6.0	Xiang et al. (2017)
Magnetic halloysite nanotubes/manganese oxide	59.9	6.0	Afzali and Fayazi (2016)
Multi-walled carbon nanotubes/manganese oxide	19.97	6.0	Salam (2013)
Magnesium–aluminum layered double hydroxides/manganese dioxide	49.87	4	Bo et al. (2015)
Hierarchical porous magnetic boehmite	84.11	–	Yang et al. (2013)
Carbomethoxy-functionalized metal–organic framework	63.052	7.0	Yu et al. (2018)
Glutamic acid/sepiolite	128.20	4.91	Karaoğlu et al. (2013)
Manganese oxide–coated zeolite	78.36	3.5	Zou et al. (2006)
Iron oxide–coated sepiolite	75.79	5.5	Eren and Gumus (2011)
Mercapto-functionalized sepiolite	151.31	–	Liang et al. (2011)
Iron oxide coated bentonite	22.20	6.0	Eren (2009)
Magnesium oxide–coated bentonite	31.86	6.0	Eren (2009)
Silica–cyanopropyl-functionalized magnetic graphene oxide	111.11	5.0	Gabris et al. (2018)
Magnetic bentonite	80.40	5	Zou et al. (2018)
Sepiolite–iron oxide–manganese dioxide nanocomposite	131.58	6.0	This work

Table 4 Thermodynamic parameters for Pb(II) adsorption on Sep–Fe_3O_4–MnO_2 nanocomposite

Temperature (K)	ΔG° (kJ mol^{-1})	ΔH° (kJ mol^{-1})	ΔS° (kJ mol^{-1} K^{-1})
288.15	− 11.33	–	–
298.15	− 11.72	16.73	0.0850
310.15	− 12.20	–	–
323.15	− 12.71	–	–

Effects of competing ions

One of main problem that limits the performance of adsorbents in practical applications is the ion selectivity of the adsorbent (Kong et al. 2017). Fig. S4 shows the effect of coexisting ions including Na^+, K^+, Ca^{2+}, Mg^{2+}, Zn^{2+}, Co^{2+}, Cd^{2+}, Ni^{2+}, Cl^-, NO_3^-, and CO_3^{2-} on the adsorption of lead ions by the Sep–Fe_3O_4–MnO_2 nanocomposite. The experimental tests were performed in a binary system containing 0.25 mmol L^{-1} of Pb(II) ion and the same concentration of each competing ion. The obtained results show that the coordination tendency for Pb(II) ions is only slightly affected in the presence of other coexisting ions, revealing the proper selectivity of the proposed sorbent material for lead removal.

Application of Sep–Fe_3O_4–MnO_2 nanocomposite in acid mine drainage treatment

The acid mine drainage (AMD) samples were collected from Tabas Parvardeh Coal Processing (Tabas, Iran) and Kushk Lead Mine (Yazd, Iran). The characteristics of both water samples are given in Table 5. The AMD samples were filtered by nylon membrane (0.45 μm) to remove particulates and the pH values were adjusted at 6.0 for adsorption experiments. After treating the AMD samples with Sep–Fe_3O_4–MnO_2 nanocomposite (2 g L^{-1}) for 60 min, FAAS analysis indicated that the lead content in all samples dropped to less than 0.1 mg L^{-1}. The removal percentage was found to be 99.1 for coal processing sample and 98.8 for lead mine sample. The above experiments prove that the prepared magnetic sorbent is more suitable for the removal of Pb(II) ions in real water samples.

Table 5 Characteristics of AMD samples

Lead mine		Coal processing	
pH	1.9	pH	5.1
Pb^{2+} (mg L^{-1})	8.66	Pb^{2+} (mg L^{-1})	2.58
Zn^{2+} (mg L^{-1})	6.10	Mg^{2+} (mg L^{-1})	4.36
Ca^{2+} (mg L^{-1})	3.42	Sb^{3+} (mg L^{-1})	1.72
Al^{3+} (mg L^{-1})	0.96	Fe^{3+} (mg L^{-1})	1.48

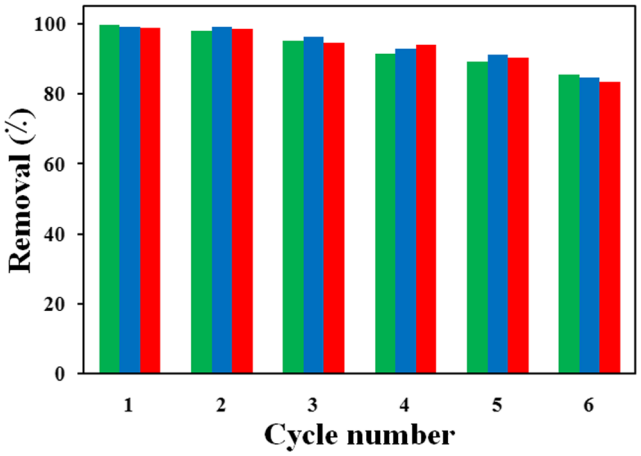

Fig. 5 Reusability and reproducibility of Sep–Fe_3O_4–MnO_2 nanocomposite between six adsorption–desorption cycles at three different batches (upon treatment with 0.1 M EDTA)

Reusability study of the adsorbent

From an economic point of view, the recyclability of an adsorbent is a very important parameter. The reproducibility of adsorbent is also very important. Thus, the parallel desorption experiments were accomplished and the removal percentages were compared. As observed in Fig. 5, the removal efficiency decreases as the number of cycle times rise. Moreover, a high desorption efficiency of Pb(II) is probably due to the strong affinity between Pb(II) and EDTA (log $K \approx 18.0$) (Madadrang et al. 2012). In addition, The Sep–Fe_3O_4–MnO_2 nanocomposite retains 90% of its initial adsorption behavior toward Pb(II) after six regeneration cycles. The decrease in adsorption performance can be attributed to the blocking of binding sites by unreleased lead ions. In addition, three parallel experiments with the same adsorbent material exhibit acceptable reproducibility. The results demonstrate that the prepared Sep–Fe_3O_4–MnO_2 nanocomposite is an effective, economical, and recyclable adsorbent.

Conclusion

In summary, a novel magnetic Sep–Fe_3O_4–MnO_2 nanocomposite was designed and synthesized for Pb(II) adsorption. Notably, the resulting adsorbent material demonstrated fast kinetics and extraordinary adsorption capacity. The ion exchange and electrostatic attraction are the contributions to the effective removal of Pb(II) ions. The adsorption process follows Langmuir isotherm model and obey the pseudo-second-order kinetic model. More significantly, besides good adsorption and rapid kinetics, the Sep–Fe_3O_4–MnO_2 nanocomposite possesses facile synthesis, excellent reusability, and easy magnetic separation, which guarantee its application in practical remediation. The combination of nanosized MnO_2

with high surface area of the magnetic Sep composite obtains an attractive chance for offering an efficient adsorbent in decontamination of polluted water.

References

Afzali D, Fayazi M (2016) Deposition of MnO_2 nanoparticles on the magnetic halloysite nanotubes by hydrothermal method for lead (II) removal from aqueous solutions. J Taiwan Inst Chem Eng 63: 421–429

Ali I (2012) New generation adsorbents for water treatment. Chem Rev 112:5073–5091

Arshadi M, Soleymanzadeh M, Salvacion J, SalimiVahid F (2014) Nanoscale zero-valent iron (NZVI) supported on sineguelas waste for Pb (II) removal from aqueous solution: kinetics, thermodynamic and mechanism. J Colloid Interface Sci 426:241–251

Babić B, Milonjić S, Polovina M, Čupić S, Kaludjerović B (2002) Adsorption of zinc, cadmium and mercury ions from aqueous solutions on an activated carbon cloth. Carbon 40:1109–1115

Barrett EP, Joyner LG, Halenda PP (1951) The determination of pore volume and area distributions in porous substances. I. Computations from nitrogen isotherms. J Am Chem Soc 73:373–380

Bo L, Li Q, Wang Y, Gao L, Hu X, Yang J (2015) One-pot hydrothermal synthesis of thrust spherical Mg–Al layered double hydroxides/MnO_2 and adsorption for Pb (II) from aqueous solutions. J Environ Chem Eng 3:1468–1475

Bowman N, Patel D, Sanchez A, Xu W, Alsaffar A, Tiquia-Arashiro SM (2018) Lead-resistant bacteria from Saint Clair River sediments and Pb removal in aqueous solutions. Appl Microbiol Biotechnol 102: 2391–2398

Celis R, Hermosin MC, Cornejo J (2000) Heavy metal adsorption by functionalized clays. Environ Sci Technol 34:4593–4599

Chandra V, Park J, Chun Y, Lee JW, Hwang I-C, Kim KS (2010) Water-dispersible magnetite-reduced graphene oxide composites for arsenic removal. ACS Nano 4:3979–3986

Chanthapon N, Sarkar S, Kidkhunthod P, Padungthon S (2018) Lead removal by a reusable gel cation exchange resin containing nanoscale zero valent iron. Chem Eng J 331:545–555

Chegrouche S, Mellah A, Barkat M (2009) Removal of strontium from aqueous solutions by adsorption onto activated carbon: kinetic and thermodynamic studies. Desalination 235:306–318

Choudhury PR, Majumdar S, Sahoo GC, Saha S, Mondal P (2018) High pressure ultrafiltration CuO/hydroxyethyl cellulose composite ceramic membrane for separation of Cr (VI) and Pb (II) from contaminated water. Chem Eng J 336:570–578

Cornejo J, Hermosin MC (1998) Structural alteration of sepiolite by dry grinding. Clay Minerals23:391-398

Doğan M, Turhan Y, Alkan M, Namli H, Turan P, Demirbaş Ö (2008) Functionalized sepiolite for heavy metal ions adsorption. Desalination 230:248–268

Du Y, Zheng G, Wang J, Wang L, Wu J, Dai H (2014) MnO_2 nanowires in situ grown on diatomite: highly efficient absorbents for the removal of Cr (VI) and As (V). Microporous Mesoporous Mater 200:27–34

Duan S, Tang R, Xue Z, Zhang X, Zhao Y, Zhang W, Zhang J, Wang B, Zeng S, Sun D (2015) Effective removal of Pb (II) using magnetic $Co_{0.6}Fe_{2.4}O_4$ micro-particles as the adsorbent: Synthesis and study on the kinetic and thermodynamic behaviors for its adsorption. Colloids Surf A Physicochem Eng Asp 469:211–223

Eren E (2009) Removal of lead ions by Unye (Turkey) bentonite in iron and magnesium oxide-coated forms. J Hazard Mater 165:63–70

Eren E, Gumus H (2011) Characterization of the structural properties and Pb (II) adsorption behavior of iron oxide coated sepiolite. Desalination 273:276–284

Fayazi M, Ghanei-Motlagh M, Taher MA (2015) The adsorption of basic dye (Alizarin red S) from aqueous solution onto activated carbon/γ-Fe_2O_3 nano-composite: kinetic and equilibrium studies. Mater Sci Semicond Process 40:35–43

Fu F, Wang Q (2011) Removal of heavy metal ions from wastewaters: a review. J Environ Manag 92:407–418

Fu R, Yang Y, Xu Z, Zhang X, Guo X, Bi D (2015) The removal of chromium (VI) and lead (II) from groundwater using sepiolite-supported nanoscale zero-valent iron (S-NZVI). Chemosphere 138:726–734

Gabris MA, Jume BH, Rezaali M, Shahabuddin S, Nodeh HR, Saidur R (2018) Novel magnetic graphene oxide functionalized cyanopropyl nanocomposite as an adsorbent for the removal of Pb (II) ions from aqueous media: equilibrium and kinetic studies. Environ Sci Pollut Res 25:27122–27,132

Ghorbani M, Shams A, Seyedin O, Lahoori NA (2018) Magnetic ethylene diamine-functionalized graphene oxide as novel sorbent for removal of lead and cadmium ions from wastewater samples. Environ Sci Pollut Res 25:5655–5667

Giraldo L, Erto A, Moreno-Piraján JC (2013) Magnetite nanoparticles for removal of heavy metals from aqueous solutions: synthesis and characterization. Adsorption 19:465–474

Guo S, Dan Z, Duan N, Chen G, Gao W, Zhao W (2018) Zn (II), Pb (II), and Cd (II) adsorption from aqueous solution by magnetic silica gel: preparation, characterization, and adsorption. Environ Sci Pollut Res 25:30938–30948

Han R, Zou W, Zhang Z, Shi J, Yang J (2006) Removal of copper (II) and lead (II) from aqueous solution by manganese oxide coated sand. I Characterization and kinetic study J Hazard Mater 137:384–395

Hayes K, Leckie J (1987) Modeling ionic strength effects on cation adsorption at hydrous oxide/solution interfaces. J Colloid Interface Sci 115:564–572

He J, Wang M, Wang W, Miao R, Zhong W, Chen S-Y, Poges S, Jafari T, Song W, Liu J (2017) Hierarchical mesoporous NiO/MnO_2@PANI core–shell microspheres, highly efficient and stable bifunctional electrocatalysts for oxygen evolution and reduction reactions. ACS Appl Mater Interfaces 9:42676–42642 687

Karaoğlu MH, Kula İ, Uğurlu M (2013) Adsorption kinetic and equilibrium studies on removal of lead (II) onto glutamic acid/sepiolite. Clean: Soil, Air, Water 41:548–556

Karthik R, Meenakshi S (2015) Removal of Pb (II) and Cd (II) ions from aqueous solution using polyaniline grafted chitosan. Chem Eng J 263:168–177

Kong L, Li Z, Huang X, Huang S, Sun H, Liu M, Li L (2017) Efficient removal of Pb (II) from water using magnetic Fe_3S_4/reduced graphene oxide composites. J Mater Chem A 5:19333–19,342

Koulouris G (1995) Dynamic studies on sorption characteristics of ^{226}Ra on manganese dioxide. J Radioanal Nucl Chem 193:269–279

Lazarević S, Janković-Častvan I, Jovanović D, Milonjić S, Janaćković D, Petrović R (2007) Adsorption of Pb^{2+}, Cd^{2+} and Sr^{2+} ions onto natural and acid-activated sepiolites. Appl Clay Sci 37:47–57

Li L, Pan Y, Chen L, Li G (2007) One-dimensional α-MnO_2: trapping chemistry of tunnel structures, structural stability, and magnetic transitions. J Solid State Chem 180:2896–2904

Liang X, Xu Y, Sun G, Wang L, Sun Y, Sun Y, Qin X (2011) Preparation and characterization of mercapto functionalized sepiolite and their application for sorption of lead and cadmium. Chem Eng J 174:436–444

Liu H, Chen W (2015) Magnetic mesoporous imprinted adsorbent based on Fe_3O_4-modified sepiolite for organic micropollutant removal from aqueous solution. RSC Adv 5:27034–27042

Liu Y, Yan J, Yuan D, Li Q, Wu X (2013) The study of lead removal from aqueous solution using an electrochemical method with a stainless

steel net electrode coated with single wall carbon nanotubes. Chem Eng J 218:81–88
Luk CHJ, Yip J, Yuen CWM, Pang SK, Lam KH, Kan CW (2017) Biosorption performance of encapsulated candida krusei for the removal of copper (II). Sci Rep 7:2159
Madadrang CJ, Kim HY, Gao G, Wang N, Zhu J, Feng H, Gorring M, Kasner ML, Hou S (2012) Adsorption behavior of EDTA-graphene oxide for Pb (II) removal. ACS Appl Mater Interfaces 4:1186–1193
Mallakpour S, Behranvand V (2017) Water sanitization by the elimination of Cd^{2+} using recycled PET/MWNT/LDH composite: morphology, thermal, kinetic, and isotherm studies. ACS Sustain Chem Eng 5:5746–5757
Matlock MM, Howerton BS, Atwood DA (2002) Chemical precipitation of lead from lead battery recycling plant wastewater. Ind Eng Chem Res 41:1579–1582
Nqombolo A, Mpupa A, Gugushe AS, Moutloali RM, Nomngongo PN (2019) Adsorptive removal of lead from acid mine drainage using cobalt-methylimidazolate framework as an adsorbent: kinetics, isotherm, and regeneration. Environ Sci Pollut Res 26:3330–3339
Qin Q, Wang Q, Fu D, Ma J (2011) An efficient approach for Pb (II) and Cd (II) removal using manganese dioxide formed in situ. Chem Eng J 172:68–74
Salam MA (2013) Coating carbon nanotubes with crystalline manganese dioxide nanoparticles and their application for lead ions removal from model and real water. Colloids Surf A Physicochem Eng Asp 419:69–79
Sharma R, Puri A, Monga Y, Adholeya A (2014) Acetoacetanilide-functionalized Fe_3O_4 nanoparticles for selective and cyclic removal of Pb^{2+} ions from different charged wastewaters. J Mater Chem A 2: 12888–12,898
Tabak A, Eren E, Afsin B, Caglar B (2009) Determination of adsorptive properties of a Turkish Sepiolite for removal of Reactive Blue 15 anionic dye from aqueous solutions. J Hazard Mater 161:1087–1094
Tan I, Ahmad A, Hameed B (2008) Adsorption of basic dye on high-surface-area activated carbon prepared from coconut husk: equilibrium, kinetic and thermodynamic studies. J Hazard Mater 154:337–346
Tan G, Wu Y, Liu Y, Xiao D (2018) Removal of Pb (II) ions from aqueous solution by manganese oxide coated rice straw biochar A low-cost and highly effective sorbent. J Taiwan Inst Chem Eng 84:85–92
Tian N, Tian X, Ma L, Yang C, Wang Y, Wang Z, Zhang L (2015) Well-dispersed magnetic iron oxide nanocrystals on sepiolite nanofibers for arsenic removal. RSC Adv 5:25236–25,243
Tripathy SS, Bersillon J-L, Gopal K (2006) Adsorption of Cd^{2+} on hydrous manganese dioxide from aqueous solutions. Desalination 194: 11–21
Wang J, Cheng C, Yang X, Chen C, Li A (2013) A new porous chelating fiber: preparation, characterization, and adsorption behavior of Pb (II). Ind Eng Chem Res 52:4072–4082
Wei X, Sugumaran PJ, Peng E, Liu XL, Ding J (2017) Low-field dynamic magnetic separation by self-fabricated magnetic meshes for efficient heavy metal removal. ACS Appl Mater Interfaces 9:36772–36,782
Xiang B, Ling D, Lou H, Gu H (2017) 3D hierarchical flower-like nickel ferrite/manganese dioxide toward lead (II) removal from aqueous water. J Hazard Mater 325:178–188
Xu D, Tan X, Chen C, Wang X (2008) Removal of Pb (II) from aqueous solution by oxidized multiwalled carbon nanotubes. J Hazard Mater 154:407–416
Yang S, Hu J, Chen C, Shao D, Wang X (2011) Mutual effects of Pb (II) and humic acid adsorption on multiwalled carbon nanotubes/polyacrylamide composites from aqueous solutions. Environ Sci Technol 45:3621–3627
Yang X, Wang X, Feng Y, Zhang G, Wang T, Song W, Shu C, Jiang L, Wang C (2013) Removal of multifold heavy metal contaminations in drinking water by porous magnetic Fe_2O_3@AlO(OH) superstructure. J Mater Chem A 1:473–477
Yu S, Zhai L, Zhong S, Qiu Y, Cheng L, Ren X (2016) Synthesis and structural characterization of magnetite/sepiolite composite and its sorptive properties for Co (II) and Cd (II). J Taiwan Inst Chem Eng 59:221–228
Yu C, Han X, Shao Z, Liu L, Hou H (2018) High efficiency and fast removal of trace Pb (II) from aqueous solution by carbomethoxy-functionalized metal-organic framework. Cryst Growth Des 18: 1474–1482
Zhang W, Li X, Zou R, Wu H, Shi H, Yu S, Liu Y (2015) Multifunctional glucose biosensors from Fe_3O_4 nanoparticles modified chitosan/graphene nanocomposites. Sci Rep 5:11129
Zhang J, Yan Z, Ouyang J, Yang H, Chen D (2018) Highly dispersed sepiolite-based organic modified nanofibers for enhanced adsorption of Congo red. Appl Clay Sci 157:76–85
Zhao J, Liu J, Li N, Wang W, Nan J, Zhao Z, Cui F (2016) Highly efficient removal of bivalent heavy metals from aqueous systems by magnetic porous Fe_3O_4-MnO_2: adsorption behavior and process study. Chem Eng J 304:737–746
Zhou Y, Hu X, Zhang M, Zhuo X, Niu J (2013) Preparation and characterization of modified cellulose for adsorption of Cd (II), Hg (II), and acid fuchsin from aqueous solutions. Ind Eng Chem Res 52:876–884
Zou W, Han R, Chen Z, Shi J, Hongmin L (2006) Characterization and properties of manganese oxide coated zeolite as adsorbent for removal of copper (II) and lead (II) ions from solution. J Chem Eng Data 51:534–541
Zou C, Jiang W, Liang J, Sun X, Guan Y (2018) Removal of Pb (II) from aqueous solutions by adsorption on magnetic bentonite. Environ Sci Pollut Res 26:1315–1322